NOVEL DYNAMICAL MODEL FOR AN OBJECT-ORIENTED SPACE TETHER SIMULATOR

F. Rodríguez-Lucas[(1)], M. Sanjurjo-Rivo[(2)], and J. Peláez[(3)]

[(1)]*Space Dynamics Group (SDG-UPM) / Empresarios Agrupados, Magallanes, 3 28015 Madrid (Spain), +34 91309800, fernando.rodriguez.lucas@gmail.com*

[(2)]*Space Dynamics Group (SDG-UPM), Universidad Carlos III de Madrid (UC3m), Avenida de la Universidad, 30, Leganes, 28911 (Spain), +34 916248222, manuel.sanjurjo@uc3m.es*

[(3)]*Space Dynamics Group (SDG-UPM), Universidad Politécnica de Madrid (UPM), Pza. de Cardenal Cisneros, 3 28040 Madrid (Spain), +34 913366300, j.pelaez@upm.es*

Abstract:

This paper presents a novel dynamical model for space tether dynamics simulation. The proposed model discretises the cable in a number of elastic rods, which in turn are modeled as a set of equivalent masses. The orbital propagation is performed using a classical Cowell's method and also a special perturbation method. The implementation is done within the framework of EcosimPro, a multidisciplinary simulation tool. A validation of the model is carried out, as well as a case of application to the de-orbiting of a satellite using an electrodynamic tether.

Keywords: *Simulation, tether, electrodynamic, dynamical model, multi-tethered systems.*

1. Introduction

Tethers have been used in space for a number of different purposes: generation of artificial gravity, formation flying, propulsion, etc [1]. Lately, space situational awareness has fostered the study of tethers in the context of space debris mitigation and removal. Tethers are considered as parts of more complex devices such as harpoons or hooks. An additional rationale for the advance in the accurate simulation of tether dynamics is the promising capabilities of electrodynamic tethers to de-orbit a satellite efficiently [2, 3, 4]. In fact, accurate simulation of tether dynamics has been identified as a key aspect to advancing the readiness level of the electrodynamic space tethers [5]. The work presented here is intended to provide the space community with a flexible and robust simulation environment for many of the aforementioned possible applications of space tethers. The focus in this work, nonetheless, is the simulation of tethered satellites and electrodynamic tethers in particular.

The dynamics of tethered spacecraft involves nonlinear effects with coupling effects between orbital motion, longitudinal, and lateral modes. Different approaches have been considered in the literature to address the simulation of space tethers: geometric numerical integration, finite elements method, and assumed modes method [5]. Nevertheless, there is still a need to simulate the dynamical behavior with required accuracy and an acceptable time consumption, as well as modeling flexibility for simulating different complex tethered configurations or with different accuracy levels. This work is intended to fulfill this need using a new tether dynamical model and non-casual and object-oriented modeling.

The space tether system is described in terms of a number of elastic rods, joined by ideal joints.

The end masses can be modeled as point masses or rigid bodies. The proposed formulation allows modeling several tethers joined to a same spacecraft. In turn, the flexibility of the non-casual modeling technique allows us to obtain robust mathematical models for complex physical systems.

A prototype library for the simulation of space tether systems has been developed for the multidisciplinary EcosimPro simulation tool. The core of the library is the orbit propagator of the masses, based on DROMO method [6], although Cowell's method can also be used. Common space dynamics capabilities are also included as spacecraft attitude dynamics and control. In this way, it is possible to simulate the whole tethered satellite system within a single simulation framework, including other coupled systems as control or power systems.

A validation is performed using examples from the literature and experimental results when available. Finally, a full de-orbiting mission of an electrodynamic tethered system is presented.

2. Tether physical model

In this work, we develop a new formulation for the simulation of space tethered systems. This formulation allows us to simulate tether systems consisting of two point masses joined by a flexible tether, but also several tethers connected to a central point mass or to a central rigid body with flying wheels. The basic component of such models is a tether with a free end and a point mass joined to the other one. The formulation for such a tether model is developed in 2.2..

Let's consider a massive, flexible (no bending resistance), and extensible tether with natural length L_u and mass m_t. We assume that the torsional effects are negligible, and a strain-tension relation linear on the extension and extension velocity [7]:

$$T = E\epsilon + D\dot{\epsilon} \tag{1}$$

The proposed model is based on physical discretization of the tether, which is described as a (selectable, n) number of massive, cylindrical and longitudinally elastic rods, joined by ideal joints.

From a dynamical point of view, each bar is considered as an equivalent dynamic system composed of two masses joined with a spring-dashpot system (hereafter, TMED). The position of the masses and the characteristics of the spring are selected so that the equivalent system reproduces exactly the transversal moment of inertia, and the deformation under external solicitations, of the original elastic bar. The equivalent system is designed in such a way that its governing equations (momentum and angular momentum) coincide with the original elastic rod governing equations. This way, the motion of an isolated bar can be described by means of the momentum equations of the two masses subject to an equivalent system of forces, or the momentum equation for the center of mass of the bar plus an attitude-like equation. This equivalent model and the equations describing its motion are described in 2.1.

Based on the proposed tether segment model, the model for a tether with a free end and an ending point mass is presented in 2.2.. In the subsequent sections, the equations for the simulation of two point masses tether systems (2.3.), hub-and-spoke multi-tethered systems (2.4.) and hub-and-spoke multi-tethered systems with central rigid body (2.5.) are presented.

2.1. Tether element model: Two-mases equivalent dashpot (TMED)

Let's consider the ith rod, which mass is m_i and its unstretched and stretched lengths are L_{u_i} and L_{a_i}, respectively. Its equivalent TMED consists of two equal masses $m_{1,i}$ and $m_{2,i}$ ($m_{1,i} = m_{2,i} = \frac{m_i}{2}$), joined by a spring-dashpot system, which constants are k_{m_i} and D_{m_i}. Aligned with the masses, there are two massless rods joining each mass with the ends A_i and B_i of the bar. The length of the massless rods is variable, so that the length of the stretched TMED, L_{a_i}, is equal to that of the original elastic bar.

Let's call d_i the distance between each mass and the center of mass (G_i) of the system (which, as in the case of the original elastic rod, is placed in the midpoint of the system), and

$$\epsilon_i = \frac{L_{a_i} - L_{u_i}}{L_{u_i}} \tag{2}$$

the deformation of the system. In the TMED, the lengths of the massless rods are chosen so that the relation between d_i and the deformation is:

$$d_i = \frac{L_{a_i}}{2\sqrt{3}} = \frac{L_{u_i}}{2\sqrt{3}}\left(1 + \epsilon_i\right) \tag{3}$$

This way, the transversal moment of inertia of the TMED reproduces exactly the one of the elastic bar:

$$I_{G_i} = \frac{1}{12} m L_{u_i}^2 \left(1 + 2\epsilon_i + \epsilon_i^2\right) \tag{4}$$

The elastic constant of the spring and its natural length are chosen to be

$$k_{m_i} = \sqrt{3}\frac{EA}{L_{u_i}} \qquad l_{N_i} = \frac{L_{u_i}}{\sqrt{3}} \tag{5}$$

being E the Young's modulus of the tether's material, and A the cross section of the wire.

Equation 3 and Eq. 5 ensure that when the TMED is stretched with a traction force applied T on its ends, its deformation and the accumulated elastic energy coincide with those of the elastic bar in the same conditions.

Since the cross section of the bar is considered negligible, the system has 6 degrees of freedom, which defines its position and orientation in space and its deformation. Hence, its state can be defined by means of the coordinates of two different points of the system, e.g., the coordinates of the two equivalent masses. Let $\boldsymbol{r}_{1,i}$ and $\boldsymbol{r}_{2,i}$ be the position vector of $m_{1,i}$ and $m_{2,i}$ with respect to an inertial reference frame $Ex_1y_1z_1$. The position of the center of mass G_i is

$$\boldsymbol{r}_{G_i} = \frac{1}{m}\left(m_1\,\boldsymbol{r}_{1,i} + m_2\,\boldsymbol{r}_{2,i}\right) = \frac{1}{2}\left(\boldsymbol{r}_{1,i} + \boldsymbol{r}_{2,i}\right) \tag{6}$$

Let's call $\boldsymbol{d}_i$ the relative position vector of the mass m_2 with respect G_i

$$\boldsymbol{d}_i = \left(\boldsymbol{r}_{2,i} - \boldsymbol{r}_{G_i}\right) \tag{7}$$

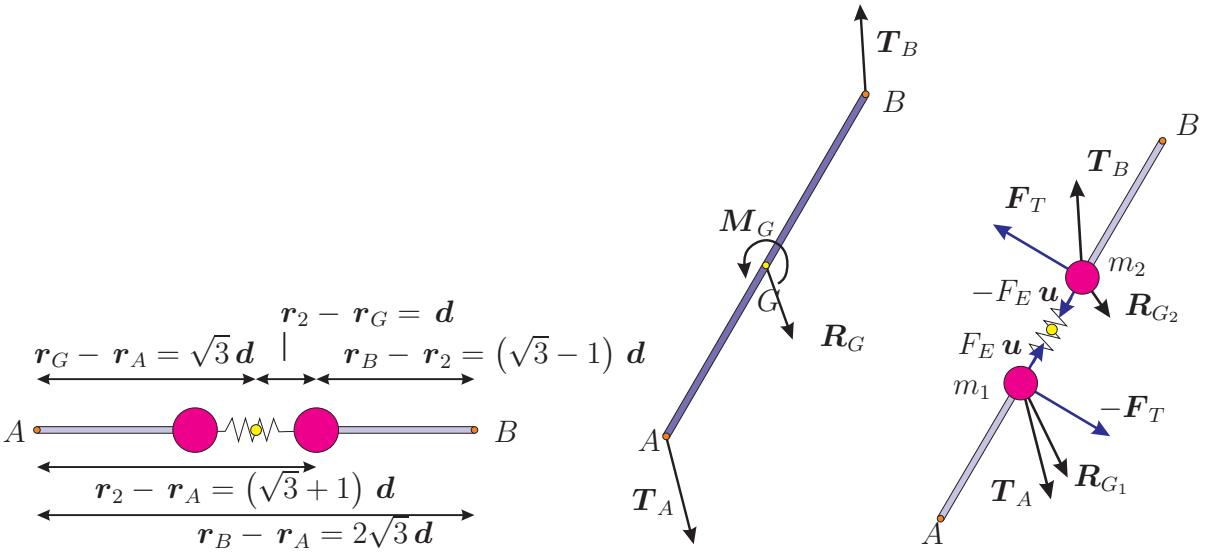

Figure 1. TMED: Relative position vectors (left) and original and equivalent forces systems (right)

This vector contains information regarding the length and orientation of the bar: its modulus is d_i, which is directly related with the deformation of the bar through Equation 3, and the unitary vector $\boldsymbol{u}_i$, aligned with the bar, defines its orientation:

$$\boldsymbol{u}_i = \frac{\boldsymbol{d}_i}{d_i} \tag{8}$$

The position and orientation of the TMED can also be described by the position vector of some of its points, and the vector $\boldsymbol{d}_i$; Fig. 2.1. summarises some expressions for the relative position vectors in terms of $\boldsymbol{d}_i$.

On the ith rod in which the tether is discretized, a distributed system of forces (due to the spherical gravitational force and perturbations) is being applied, with total value $\boldsymbol{R}_i = \int_{A_i}^{B_i} \boldsymbol{R}_i^{dm} dm$ and moment with respect G_i $\boldsymbol{M}_{G_i}$, and the reaction point forces applied on the ends of the bar $\boldsymbol{T}_{A_i}$ and $\boldsymbol{T}_{B_i}$, due to the action of the rest of the tether over the segment considered. The governing equations for the motion of the center of mass and for the attitude motion of the elastic bar, are:

$$m_i\,\ddot{\boldsymbol{r}}_{G_i} = \boldsymbol{R}_i + \boldsymbol{T}_{A,i} + \boldsymbol{T}_{B,i} \tag{9}$$

$$\frac{d\boldsymbol{H}_{G_i}}{dt} = \boldsymbol{M}_{G_i} + \frac{L_{a_i}}{2}\,\boldsymbol{u} \times (\boldsymbol{T}_{B,i} - \boldsymbol{T}_{A,i}) \tag{10}$$

It is possible to find a combination of point forces which, when applied on the equivalent masses of the TMED, obtains an equivalent equations system equivalent to that of the original elastic bar Eq. 9-10.

To obtain the equivalent set of equations, it is necessary to apply, on the mass m_1 (on m_2):

- The total of the distributed forces along the corresponding half-bar: $\boldsymbol{R}_{1,i} = \int_{A_i}^{G_i} \boldsymbol{R}_i^{dm} dm$ ($\boldsymbol{R}_{2,i} = \int_{G_i}^{B_i} \boldsymbol{R}_i^{dm} dm$ on m_2)
- The internal force $F_{E_i}\,\boldsymbol{u}$ due to the spring ($-F_{E_i}\,\boldsymbol{u}$ on m_2)
- The reaction $\boldsymbol{T}_{A,i}$, since it is completely transmitted by the massless rod from A_i to m_1 ($\boldsymbol{T}_{B,i}$ on m_2)

- And an additional force $-\boldsymbol{F}_{T_i}$, orthogonal to $\boldsymbol{u}_i$ ($\boldsymbol{F}_{T_i}$ on m_2) so that the moment of the whole system of forces with respect G_i coincides with the total moment acting on the original bar. Note that the total value of the pair of forces is null. From the previous condition, an expression for $\boldsymbol{F}_{T_i}$ can be obtained:

$$\boldsymbol{F}_T = \boldsymbol{F}_{T_P} + \boldsymbol{F}_T^* \tag{11}$$

being

$$\boldsymbol{F}_T^* = \frac{\sqrt{3}-1}{2}\,\bar{\bar{\mathbf{J}}}(\,\boldsymbol{u}) \circ (\boldsymbol{T}_B - \boldsymbol{T}_A) \tag{12}$$

and

$$\boldsymbol{F}_{T_P} = -\frac{1}{2d}\left[\,\boldsymbol{u} \times \boldsymbol{M}_{G_\perp} + d\,\bar{\bar{\mathbf{J}}}(\,\boldsymbol{u}) \circ (\boldsymbol{R}_{G_2} - \boldsymbol{R}_{G_1})\right] \tag{13}$$

Here,

$$\boldsymbol{M}_{G_\perp} = -\,\boldsymbol{u} \times (\,\boldsymbol{u} \times \boldsymbol{M}_G) \tag{14}$$

is the component of the moment of $\boldsymbol{M}_G$ orthogonal to the vector $\boldsymbol{u}$.

The term $\boldsymbol{F}_{T_P}$ can then be obtained adding the contribution of the different forces acting on the tether segment: $\boldsymbol{F}_{T_P} = \boldsymbol{F}_{T_g} + \boldsymbol{F}_{T_{ed}} + \boldsymbol{F}_{T_{aero}} \ldots$

The tensor $\bar{\bar{\mathbf{J}}}(\,\boldsymbol{u})$, which removes the parallel component of the vector $\boldsymbol{x}$ to which it is applied, is defined as:

$$\bar{\bar{\mathbf{J}}}(\,\boldsymbol{u}) = \bar{\bar{I}} - [\,\boldsymbol{u},\,\boldsymbol{u}] \qquad \text{so that} \qquad \bar{\bar{\mathbf{J}}}(\,\boldsymbol{u}) \circ \boldsymbol{x} = -\,\boldsymbol{u} \times (\,\boldsymbol{u} \times \boldsymbol{x}) \tag{15}$$

The motion of the bar can be described then by the momentum equations of the TMED masses subject to the equivalent set of forces:

$$m_{1,i}\frac{d^2\,\boldsymbol{r}_{1,i}}{dt^2} = \boldsymbol{R}_{1,i} + \boldsymbol{T}_{i,A} + F_{i,E}\,\boldsymbol{u}_i - \boldsymbol{F}_{T,i} \tag{16}$$

$$m_{2,i}\frac{d^2\,\boldsymbol{r}_{2,i}}{dt^2} = \boldsymbol{R}_{2,i} + \boldsymbol{T}_{i,B} - F_{i,E}\,\boldsymbol{u}_i + \boldsymbol{F}_{T,i} \tag{17}$$

It is possible to obtain an equivalent set of equations; from the addition of Eq. 16 and Eq.17, the momentum equation of the whole system is obtained

$$m_i\frac{d^2\,\boldsymbol{r}_{G,i}}{dt^2} = (\boldsymbol{R}_{2,i} + \boldsymbol{R}_{1,i}) + (\boldsymbol{T}_{i,B} + \boldsymbol{T}_{i,A}) \tag{18}$$

and from the substraction of the equations, a second order differential equation is obtained for vector $\boldsymbol{d}$, which governs the attitude motion and deformation evolution of the bar:

$$m_i\,\ddot{\boldsymbol{d}}_i = (\boldsymbol{R}_{2,i} - \boldsymbol{R}_{1,i}) - 2F_{i,e}\,\boldsymbol{u} + 2\boldsymbol{F}_{T,i}^* + \bar{\bar{\mathbf{J}}}_2(\,\boldsymbol{u}_i) \circ (\boldsymbol{T}_{i,B} - \boldsymbol{T}_{i,A}) \tag{19}$$

being

$$\bar{\bar{\mathbf{J}}}_2(\,\boldsymbol{u}_i) = \bar{\bar{\mathbf{I}}} - \left(\sqrt{3}-1\right)\bar{\bar{\mathbf{J}}}(\,\boldsymbol{u}_i) \tag{20}$$

Note that Eq. 18 coincides with the momentum equation of the original elastic bar (Eq. 9). The moment equation of the original elastic bar (Eq. 10) can be obtained (after some algebra) from Eq. 19 by taking the vectorial product with respect to $\boldsymbol{u}$.

2.2. Tether with a free end and a point mass m_f. Reaction forces calculation

As a first step for the modeling of the whole tethered space system, we focus now in the model of a tether with a free end and a point ending mass, m_f, at $\boldsymbol{r}_f$. The tether is modeled as n TMED joined to the adjacent bars by means of ideal joints.

The $3n$ restrictions associated with the n joints

$$\boldsymbol{r}_{B,i} = \boldsymbol{r}_{A,i+1} \qquad i = 1, n-1 \qquad \boldsymbol{r}_f = \boldsymbol{r}_{B,n} \tag{21}$$

reduce to $3n+3$ the degrees of freedom (dof) of the system (without the joints, the system would have $6n+3$ dof), and give rise to the existence of the reactions acting in the ends of the bars, $\boldsymbol{T}_{A,i}$ and $\boldsymbol{T}_{B,i}$ $(i = 1, n)$, which are unknowns:

$$\boldsymbol{T}_{B,i} = -\boldsymbol{T}_{A,i+1} \qquad i = 1, n-1 \qquad \boldsymbol{T}_f = -\boldsymbol{T}_{B,n} \tag{22}$$

The $3n+3$ dof fix the status of the tether. Given the position of the free end with respect an inertial frame, $\boldsymbol{r}_{A,1}$, and the orientation and length of each rod, $\boldsymbol{d}_j$, the position of the joints and center of mass of the bars can be written (similar relations for the velocity and acceleration of such points can be obtaining through derivation):

$$\boldsymbol{r}_{B,i-1} = \boldsymbol{r}_{A,1} + \sum_{j=1}^{i-1} 2\sqrt{3}\,\boldsymbol{d}_j \qquad \boldsymbol{r}_{G,i} = \boldsymbol{r}_{A,1} + \sum_{j=1}^{i-1} 2\sqrt{3}\,\boldsymbol{d}_j + \sqrt{3}\,\boldsymbol{d}_i \tag{23}$$

The motion of such system is described by the motion equations of the ending mass and bars:

$$m_f\,\ddot{\boldsymbol{r}}_f = \boldsymbol{R}_f + \boldsymbol{T}_f \tag{24}$$

$$m_i\,\ddot{\boldsymbol{r}}_{G,i} = \boldsymbol{R}_{1,i} + \boldsymbol{R}_{2,i} + \boldsymbol{T}_{A,i} + \boldsymbol{T}_{B,i} \qquad i = 1, n \tag{25}$$

$$m_i\,\ddot{\boldsymbol{d}}_i = (\boldsymbol{R}_{2,i} - \boldsymbol{R}_{1,i}) - 2F_{e_i}\,\boldsymbol{u} + 2\boldsymbol{F}_{T_P,i} + \bar{\bar{\mathbf{J}}}_2(\,\boldsymbol{u}_i) \circ (\boldsymbol{T}_{B,i} - \boldsymbol{T}_{A,i}) \qquad i = 1, n \tag{26}$$

together with the constraints Eq. 21 and Eq. 22

Equations 24, 25 and 26 can be rearranged taking into account the relation of the second derivatives obtained from Eq. 23 to obtain:

$$2\sqrt{3}m_i \sum_{j=1}^{i-1} \frac{1}{m_j} \bar{\bar{\mathbf{J}}}_{2,j} \circ (\boldsymbol{T}_{B,j} - \boldsymbol{T}_{A,j}) + \left(\sqrt{3}\,\bar{\bar{\mathbf{J}}}_{2,i} - \bar{\bar{\mathbf{I}}}\right) \circ \boldsymbol{T}_{B,i} \quad - \tag{27}$$

$$- \left(\sqrt{3}\,\bar{\bar{\mathbf{J}}}_{2,i} + \bar{\bar{\mathbf{I}}}\right) \circ \boldsymbol{T}_{A,i} + m_i\, \ddot{\boldsymbol{r}}_{A,1} \;=\; \boldsymbol{\mathcal{R}}_i \qquad i = 1, n \tag{28}$$

$$2\sqrt{3}m_f \sum_{j=1}^{n} \frac{1}{m_j} \bar{\bar{\mathbf{J}}}_{2,j} \circ (\boldsymbol{T}_{B,j} - \boldsymbol{T}_{A,j}) + \boldsymbol{T}_{B,n} + m_f\, \ddot{\boldsymbol{r}}_{A,1} \;=\; \boldsymbol{\mathcal{R}}_f \tag{29}$$

Where

$$\boldsymbol{\mathcal{R}}_i \;=\; \boldsymbol{R}_i - 2\sqrt{3}m_i \sum_{j=1}^{i-1} \frac{1}{m_j} \boldsymbol{R}_j^* - \sqrt{3}\boldsymbol{R}_i^* \tag{30}$$

$$\boldsymbol{\mathcal{R}}_f \;=\; \boldsymbol{R}_f - 2\sqrt{3}m_f \sum_{j=1}^{n} \frac{1}{m_j} \boldsymbol{R}_j^* \tag{31}$$

groups the effect of all the forces on the bars (elastic and external different from the reactions). Here we have used:

$$\boldsymbol{R}_j^* = (\boldsymbol{R}_{2,j} - \boldsymbol{R}_{1,j}) - 2F_{e_j}\, \boldsymbol{u}_j + 2\boldsymbol{F}_{T_P,j} \tag{32}$$

and

$$\boldsymbol{R}_i = \boldsymbol{R}_{1,i} + \boldsymbol{R}_{2,i} \qquad \text{and} \qquad \bar{\bar{\mathbf{J}}}_{2,i} = \bar{\bar{\mathbf{J}}}_2(\, \boldsymbol{u}_i)$$

The $3n + 3$ equations Eq. 28-29 are a linear relation between the $3n + 6$ unknowns $\ddot{\boldsymbol{r}}_{A,1}$, $\boldsymbol{T}_{A,1}$, $\boldsymbol{T}_{B,j}$, and will be referred hereafter as $L(\, \ddot{\boldsymbol{r}}_{A,1}, \boldsymbol{T}_{A,1}, \boldsymbol{T}_{B,j}) = \boldsymbol{\mathcal{R}}_i$.

The motion of the tether with a free end A_1 is then described by the equations:

$$m_{2,i}\, \ddot{\boldsymbol{r}}_{2,i} \;=\; \boldsymbol{R}_{2,i} + \boldsymbol{T}_{B,i} - F_{e,i}\, \boldsymbol{u}_i + \boldsymbol{F}_{T,i} \qquad i = 1, n \tag{33}$$

$$L(\, \ddot{\boldsymbol{r}}_{A,1}, \boldsymbol{T}_{A,1}, \boldsymbol{T}_{B,j}) \;=\; \boldsymbol{\mathcal{R}}_i \tag{34}$$

Note that the mathematical problem is not yet closed, as the acceleration of the free end $\ddot{\boldsymbol{r}}_{A,1}$ is not yet known. For solving the problem, $L(\, \ddot{\boldsymbol{r}}_{A,1}, \boldsymbol{T}_{A,1}, \boldsymbol{T}_{B,j}) = \boldsymbol{\mathcal{R}}_i$ must be extended with 3 additional conditions providing $\ddot{\boldsymbol{r}}_{A,1}$ or relating it with $\boldsymbol{T}_{A,1}$ or $\boldsymbol{T}_{B,j}$. Then, the motion of the tether can be simulated solving the linear system L at each time step, and integrating the $3n$ momentum equations of the equivalent masses and that of the free end.

In the following sections we state the closed equation systems for some typical tether systems.

2.3. Tether with two end point masses

Let's consider now that the free end A_1 of the tether described in the previous section is ideally attached to a point mass m_0. This mass will be subject to the total of the external forces (gravitational, third body, etc) $\boldsymbol{R}_0$, and the reaction due to the connection of the tether $\boldsymbol{T}_0$.

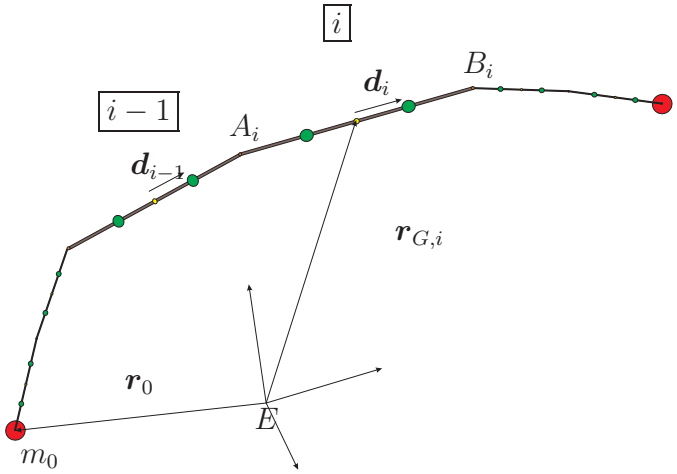

Figure 2. Tether with two end point masses model

Then, the whole set of equations describing the motion of the tether connecting the point masses m_0 and m_f are:

$$m_0\,\ddot{\boldsymbol{r}}_0 = \boldsymbol{R}_0 + \boldsymbol{T}_0 \tag{35}$$

$$\boldsymbol{r}_0 = \boldsymbol{r}_{A,1} \rightarrow \ddot{\boldsymbol{r}}_0 = \ddot{\boldsymbol{r}}_{A,1} \tag{36}$$

$$\boldsymbol{T}_0 = -\boldsymbol{T}_{A,1} \tag{37}$$

$$m_{2,j}\,\ddot{\boldsymbol{r}}_{2,j} = \boldsymbol{R}_{2,j} + \boldsymbol{T}_{B,j} - F_{e,j}\,\boldsymbol{u}_j + \boldsymbol{F}_{T,j} \qquad j = 1, n \tag{38}$$

$$L(\ddot{\boldsymbol{r}}_{A,1}, \boldsymbol{T}_{A,1}, \boldsymbol{T}_{B,j}) = \boldsymbol{\mathcal{R}}_i \tag{39}$$

This set of equation can be split in three parts:

- The motion equation of the mass m_0, Eq. 35
- The connection equations, representing the ideal constraints, Eq. 36 and Eq. 37
- The motion equations of the tether with the ending mass m_f, Equations 38-39

Note that Eq. 35 couples with Eq. 39 giving a linear system of size $3n+6$ $L_{2m}(\ddot{\boldsymbol{r}}_0, \boldsymbol{T}_{A,1}, \boldsymbol{T}_{B,j}) = \boldsymbol{\mathcal{R}}_{2m,i}$, that must be solved each time step during the integration of the momentum equations.

2.4. Point mass m_0 with several connected tethers

Let's consider now a hub-and-spoke (HAS) multi-tethered system, consisting in a central point mass m_0 to which N_t tethers (as the one described in 2.2.) are connected. The motion equations of such a system consist on the momentum equation of the particle m_0, and the motion equations

of each tether:

$$m_0\,\ddot{\boldsymbol{r}}_0 = \boldsymbol{R}_0 - \sum_{l=1}^{N_t} \boldsymbol{T}_{A,1}^{(l)} \tag{40}$$

$$\boldsymbol{r}_0 = \boldsymbol{r}_{A,1}^{(k)} \rightarrow \ddot{\boldsymbol{r}}_0 = \ddot{\boldsymbol{r}}_{A,1}^{(k)} \qquad k = 1, N_t \tag{41}$$

$$m_{2,j}^{(k)}\,\ddot{\boldsymbol{r}}_{2,j}^{(k)} = \boldsymbol{R}_{2,j}^{(k)} + \boldsymbol{T}_{B,j}^{(k)} - F_{e,j}^{(k)}\,\boldsymbol{u}_j^{(k)} + \boldsymbol{F}_{T,j}^{(k)} \qquad j = 1, n \tag{42}$$

$$L(\,\ddot{\boldsymbol{r}}_{A,1}^{(k)}, \boldsymbol{T}_{A,1}^{(k)}, \boldsymbol{T}_{B,j}^{(k)}) = \boldsymbol{\mathcal{R}}_i^{(k)} \tag{43}$$

Now all the linear systems of the tethers couples into a bigger linear system $L_{HAS}(\,\ddot{\boldsymbol{r}}_0, \boldsymbol{T}_{A,1}^{(k)}, \boldsymbol{T}_{B,j}^{(k)}) = \boldsymbol{\mathcal{R}}_{HAS,i}^{(k)}$ of size $N_T(n+3)+3$. that must be solved each time step for obtaining the reaction forces.

2.5. Rigid body with several connected tethers

The equations for the hub-and-spoke multi-tethered system can be easily adapted for taking into account the attitude dynamics of a central body. Let's assume, for example, a rigid body with N_w wheels of mass m_B, which center of mass is placed at $\boldsymbol{r}_{G_B}$ with respect to the inertial frame. Let $\bar{\bar{\mathbf{J}}}_B$ be its inertia tensor (including the contribution of the wheels) expressed in the non-inertial B frame, attached to the center of mass G_B, which rotates with respect to the inertial frame with angular speed $\boldsymbol{\omega}_B$. The rigid body has N_t attachment points to which the tethers can be ideally joined, placed at $\boldsymbol{r}_{B,Att_k}$ with respect the B frame. The motion equations of such system are ([8], [9]):

$$m_B\,\ddot{\boldsymbol{r}}_{G_B} = \boldsymbol{R}_B - \sum_{k=1}^{N_t} \boldsymbol{T}_{A,1}^{(k)} \tag{44}$$

$$\bar{\bar{\mathbf{J}}}_B\dot{\boldsymbol{\omega}}_B = \boldsymbol{M}_{G_B} - \dot{\boldsymbol{h}}_w - \boldsymbol{\omega}_B \times \left(\bar{\bar{\mathbf{J}}}_B\boldsymbol{\omega}_B + \boldsymbol{h}_w\right) - \sum_{k=1}^{N_{Att}} \boldsymbol{r}_{B,Att_k} \times \boldsymbol{T}_{A,1}^{(k)} \tag{45}$$

$$\dot{\boldsymbol{h}}_w = \boldsymbol{M}_w \tag{46}$$

Now, due to the attitude dynamics, the geometrical constraints of the attachments (the connection equations spacecraft-tethers) are more complex than in the previous cases. Assuming that the attachment points are fixed with respect the body frame B:

$$\boldsymbol{r}_{B,Att_k} = \boldsymbol{r}_{A,1}^{(k)} \rightarrow \ddot{\boldsymbol{r}}_{B,Att_k} = \ddot{\boldsymbol{r}}_{G_B} + \boldsymbol{\omega} \times (\boldsymbol{\omega} \times \boldsymbol{r}_{B,Att_k}) + \dot{\boldsymbol{\omega}} \times \boldsymbol{r}_{B,Att_k} = \ddot{\boldsymbol{r}}_{A,1}^{(k)} \tag{47}$$

The motion equations of each attached tether are:

$$m_{2,j}^{(k)}\,\ddot{\boldsymbol{r}}_{2,j}^{(k)} = \boldsymbol{R}_{2,j}^{(k)} + \boldsymbol{T}_{B,j}^{(k)} - F_{e,j}^{(k)}\,\boldsymbol{u}_j^{(k)} + \boldsymbol{F}_{T,j}^{(k)} \qquad j = 1, n \tag{48}$$

$$0 = L(\,\ddot{\boldsymbol{r}}_{A,1}^{(k)}, \boldsymbol{T}_{A,1}^{(k)}, \boldsymbol{T}_{B,j}^{(k)}) \tag{49}$$

For the integration of the motion equations Eq. (44), (45), (46), (48) it is needed now to solve a bigger linear system for obtaining the reactions on the ends of the bars, the acceleration of the center of masses of the spacecraft and the rotational acceleration of the spacecraft:

$$L_{RB}(\ddot{\boldsymbol{r}}_{G_B}, \dot{\boldsymbol{\omega}}_B, \boldsymbol{T}^{(k)}_{A,1}, \boldsymbol{T}^{(k)}_{B,j}) = \boldsymbol{\mathcal{R}}^{(k)}_{RB,i}$$

2.6. Orbit propagation

The methods presented in the previous section involve the computation of the trajectory of one or several particles, under the influence of a set of forces, representing the external forces applied on the tether (gravitational, perturbations) or internal (elastic, reactions).

In orbital mechanics applications, the equations of motion that determine the motion of the particles are those of the perturbed two body problem. The sources of perturbing forces are both external and internal. A non exhaustive list of perturbations include inhomogeneous gravitational potential, electrodynamic forces, internal elastic forces, reactions due to linkages or constraints.

In this work, two methods were tested for the computation of the particle trajectories. Firstly, Cowell's method [10] was implemented as a reference approach. This is a classical formulation based on the direct integration of the momentum equation of the particle expressed in rectangular coordinates in a inertial reference. Secondly, a special perturbations method, DROMO [6] has been implemented. This formulation is based on the variation of the parameters and Hansen's concept of the ideal frame [11] and it is expected to show better computational performance. Details on the specific implementation of these methods into the library can be found in future publications.

3. The Space Flight Dynamics and Space Tether simulation libraries

Based on the formulation described in the previous sections, a set of simulation libraries have been developed in the tool EcosimPro for the simulation of space tether systems and general space dynamics applications. Both, the presented physical formulation and the libraries, have been developed taking maximum advantage of the object-oriented and non-causal modeling paradigms [12] available in EcosimPro.

3.1. EcosimPro

EcosimPro [13], [12] is a multidisciplinary modeling and simulation environment. It is extensively used by the space industry for the simulation of liquid, solid and hybrid space propulsion systems [14], spacecraft power systems [15] space electrical propulsion systems, and, more recently, space dynamics applications [16].

In the context of EcosimPro, the so-called *components* contain a mathematical description of the corresponding real world component. Components can communicate with each other through the *ports*, which define the set of variables to be interchanged between the connected components. This way, complex systems can be graphically modeled by drag-and-dropping the required components

and connecting them. Once the model is finished, the tool automatically compiles all the equations of the different components and the *connection equations* coming from the connected ports, and creates a closed mathematical equation system after arranging the equations based on internal algorithms [12], [17]. During this step, it is able of to manage linear and non-linear equation systems. Once the mathematical problem is closed, different calculations can be performed, such as the integration of the resulting ODE or DAE system, the calculation of steady solutions, or optimization calculations with the included solvers (e.g. DASSL, Powell's hybrid method, etc). The tool is flexible enough for using external solvers or creating specific calculations.

3.2. Spaceflight Dynamics and Space Tether simulation libraries

The low level functions and components included in the library for astrodynamics calculations include:

- Low level astrodynamics functions: calendar/time calculations, planetary ephemeris, space environment (gravitational field, atmosphere, magnetic field, etc), eclipse, etc. Different levels of detail can be selected depending on the planet.
- Orbit propagation of one or several particles, using Cowell's method or DROMO method.
- Attitude propagation of rigid bodies with arbitrary number of momentum wheels.
- Forces and torque calculation of the different perturbation effects.

Following an object oriented approach, a set of components have been developed based on the above low level functions and components. Among others, this library includes:

- Environment component, for setting the space environment in which the satellite(s) will evolve. Different degrees of fidelity can be selected for the gravity field, magnetic field, third body ephemeris, etc
- Kepler particle, for the simulation of a keplerian orbit
- Cowell/DROMO particles, for the orbit calculation of a point mass
- Formation flying particles, for the orbit calculation of several point masses
- Rigid body with flying wheels (using Cowell/DROMO) for the spacecraft orbit and attitude motion calculation

A detailed description of the space dynamics library and its capabilities is out of the scope of the present work and will be introduced in a future publication. Additionally to these general components, the formulations described in the previous sections have been encapsulated in the components:

- Tether attachment, encapsulating the *connection* equations Eq. 36 and Eq. 37
- Tether component (Cowell/DROMO), encapsulating the equations of a tether with a free end as the one described in 2.2.
- Nail component, imposing null displacement to the component to which is connected.

This way, complex space tethered systems can be modeled by connecting the corresponding components, obtaining the equation systems described in 2.3., 2.4. or 2.5..

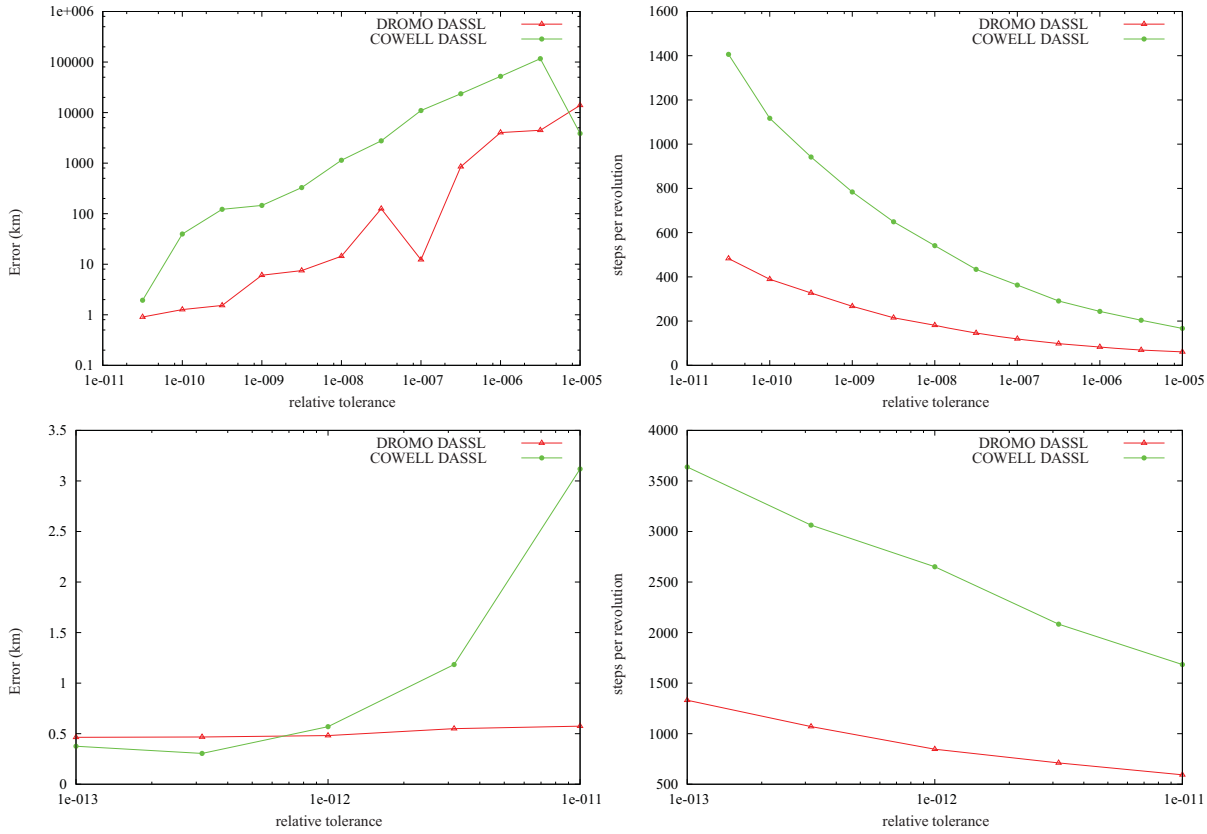

Figure 3. Stiefel problem test case. DASSL solver performances with DROMO and Cowell's methods. Left: error with respect the exact solution (52)**. Right: mean number of integration steps per orbit**

Furthermore, the space tether system model can be connected to other spacecraft subsystems, such as the control or the power system, modeled with other existing EcosimPro libraries, in order to simulate the behavior of the complete system.

4. Test cases

4.1. One mass orbit propagation. Stiefel problem

The validation of the orbital propagation core is carried out using a reference problem proposed by Stiefel & Scheifele [18]. The reference scenario consist of propagating the trajectory of a mass particle in a high eccentric ($e = 0.95$) non-equatorial ($i = 30°$) initial orbit . The mass particle is subject to lunar and J_2 perturbations. These perturbations are modeled analytically. The problem is posed as computing the position of the mass particle after 288.12768941 mean solar days (50

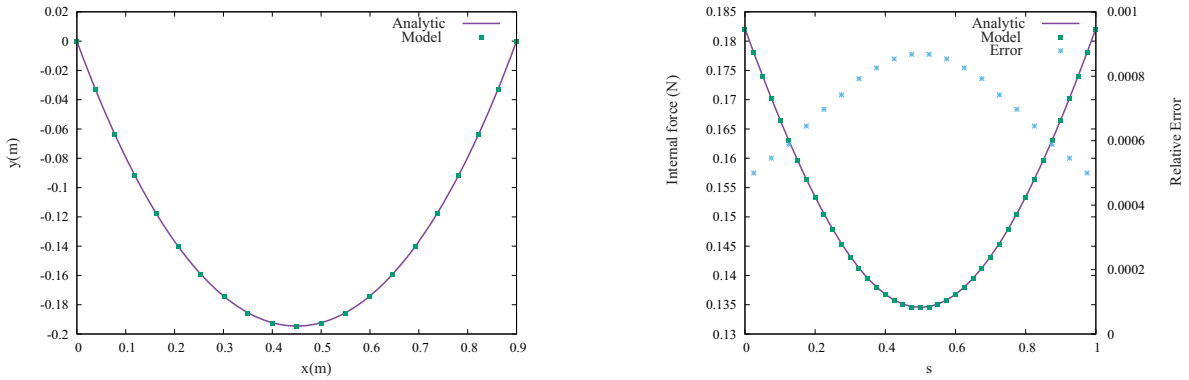

Figure 4. Tether catenary configuration (Left) and internal forces distribution (Right)

orbits), starting from the perigee of the initial orbit:

$$(x_1, y_1, z_1) = (0.0, -5888.9727, -3400.0)\ km \tag{50}$$

$$(\dot{x}_1, \dot{y}_1, \dot{z}_1) = (10.691338, 0.0, 0.0)\, km\, s^{-1} \tag{51}$$

In [18], a detailed description of the problem can be consulted. As an accurate result, the following solution is given in the aforementioned reference:

$$(x_{1f}, y_{1f}, z_{1f}) = (-24219.0503, 227962.1064, 129753.4424)\, km \tag{52}$$

This result was obtained with 498 integration steps per orbit. This solution is used to measure the performance of the propagation methods. The metric of quality is the distance from the final position obtained by integration and the reference solution (52).

Figure 4.1. shows the performances of DASSL integrator with Cowell's and DROMO methods. DROMO offers more accuracy (error propagation in Cowell is exponential) and lower computational cost. Nevertheless, DASSL integrator is less accurate and less efficient when compared to integration methods as RK7(8), when compared to previous analysis of the reference problem [6]. Therefore, the use of an *stiff* integrator such as DASSL penalises efficiency and accuracy when compared to solvers of high accuracy as RK7(8). It is fair to pay this toll because DASSL is capable of managing stiff problems. It is advisable, however, to carry out a detailed study comparing integrators with other test cases in the future.

For the orbit propagation of several particles, a set of trusted results was generated using the already tested one-particle propagator for different initial conditions for each particle. Then, the trajectory of the particles was calculated with the specific flight formation component, and compared with the trusted results, achieving a good accuracy for all the particles.

4.2. Stationary solutions: catenary

The flexibility of the formulation and the non-causal modeling allow defining test cases for which an analytical solution or experimental results are known. This is the case of the catenary steady solution.

Firstly, for the simulation of a pendulum, we extend the formulation of the tether with the condition of a steady free end:

$$\begin{aligned} \ddot{\boldsymbol{r}}_0 &= 0 && (53)\\ \boldsymbol{r}_0 &= \boldsymbol{r}_{A,1} \rightarrow \ddot{\boldsymbol{r}}_0 = \ddot{\boldsymbol{r}}_{A,1} && (54)\\ m_{2,i}\,\ddot{\boldsymbol{r}}_{2,i} &= \boldsymbol{R}_{2,i} + \boldsymbol{T}_{B,i} - F_{e,i}\,\boldsymbol{u}_i + \boldsymbol{F}_{T,i} \qquad i = 1, n && (55)\\ L(\ddot{\boldsymbol{r}}_{A,1}, \boldsymbol{T}_{A,1}, \boldsymbol{T}_{B,j}) &= \boldsymbol{\mathcal{R}}_i && (56) \end{aligned}$$

From the graphical modeling point of view, this set of equations are equivalent to the model obtained when the 'tether component' is connected with the 'nail component'.

In order to calculate the steady catenary solution, we must cancel the derivatives of the model, and compute the value $\boldsymbol{R}_f$ of the external force on the ending mass m_f so that its position is the one required by the user. The tool automatically rearranges the equations in order to fulfill the described conditions.

Figure 4 show the shape of the tether and the internal forces distribution (reactions and elastic forces) compared to those of the analytic formulation for a tether of length $L_0 = 1m$ and $EA = 40.06N$ when the free end and the ending mass are placed horizontally separated $0.9m$ at the Earth surface.

4.3. Test case: tether in circular orbit

For a preliminary validation of the tether in orbit, we consider now the motion of a non-conductive tether connecting two masses, one of them, m_0 being much bigger than the other one, m_f. The center of masses of this system is quite close to m_0 and it follows a keplerian orbit. In this specific case, we consider a circular orbit of radius $r_0 = 7400km$. Some characteristic phenomena of such a system were used as reference for the tether validation, for several models with different number of rods:

- When initially aligned with the local vertical, the tether continues in such relative equilibrium configuration (not showed in figures)
- When the tether is set initially straight, but forming an in-plane θ_0 angle contained in the orbital plane with the local vertical, it evolves straight in the orbital plane swinging around the local vertical with frequency $\sqrt{3}\omega$.
- When the tether is set initially straight, with an out-of-plane ϕ_0 angle with the orbital plane, the tether swings around the orbital plane with frequency 2ω.

In Fig. 4.3., some selected results are presented for the case of a two rods tether model.

Once the rigid-body oscillation modes of the tether are checked, we set the initial conditions so that the lateral modes are excited. Fig. 4.3. shows the evolution of the in-plane and out-of-plane

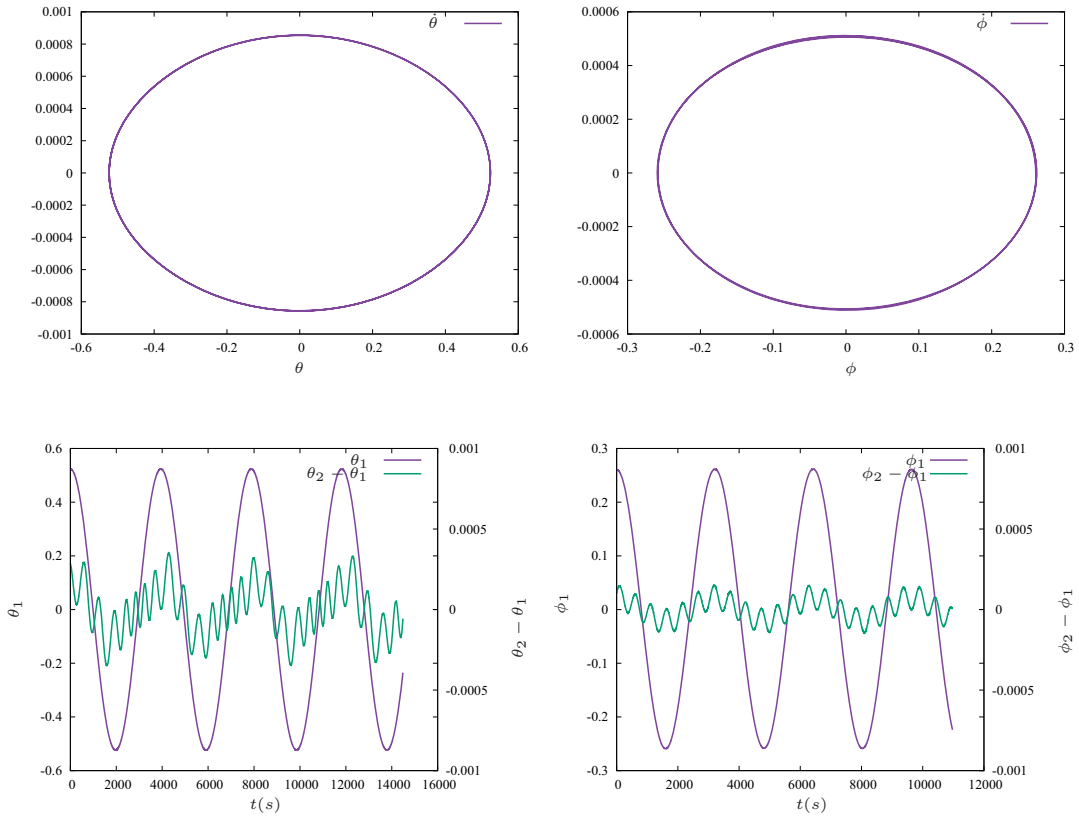

Figure 5. Two bars tether model in circular orbit. Initial conditions: Straight tether with $\theta_0 = \pi/6$, $\phi_0 = 0$ (Left) and $\theta_0 = 0$, $\phi_0 = \pi/12$ (Right)

angles for a two rods tether model, in which the higher frequency lateral modes can be observed.

5. Application case: de-orbiting a satellite with an electrodynamic tether

As an application case, we simulate now a de-orbiting mission, in which a 1063 kg satellite in an Earth circular orbit with an altitude of about 1000 km and an inclination 35^o is de-orbited by using an Aluminum tether of length $L_t = 5km$. The ending mass is $m_f = 392.2kg$, so that the tether is self-balanced [19]. In this first case, the current is set to be constant during the whole mission, $I = 2A$, and the magnetic field is modeled as a dipole aligned with the Earth's rotation axis. Fig. 7 shows the evolution of some model parameters during the mission when using a single rod tether model. The de-orbit lasts for approximately 35 days. As the orbit axis decreases, the deformation induced by the gravity gradient increases. In-plane and out-of-plane oscillations induced by the electrodynamic forces are bounded through the whole mission (self-balanced tether). The in-plane angle oscillates around a negative value.

6. Conclusions

A new formulation for the modeling of space tether systems has been developed. The tether is discretized in a number of elastic rods, and its motion can be described by motion of a set of

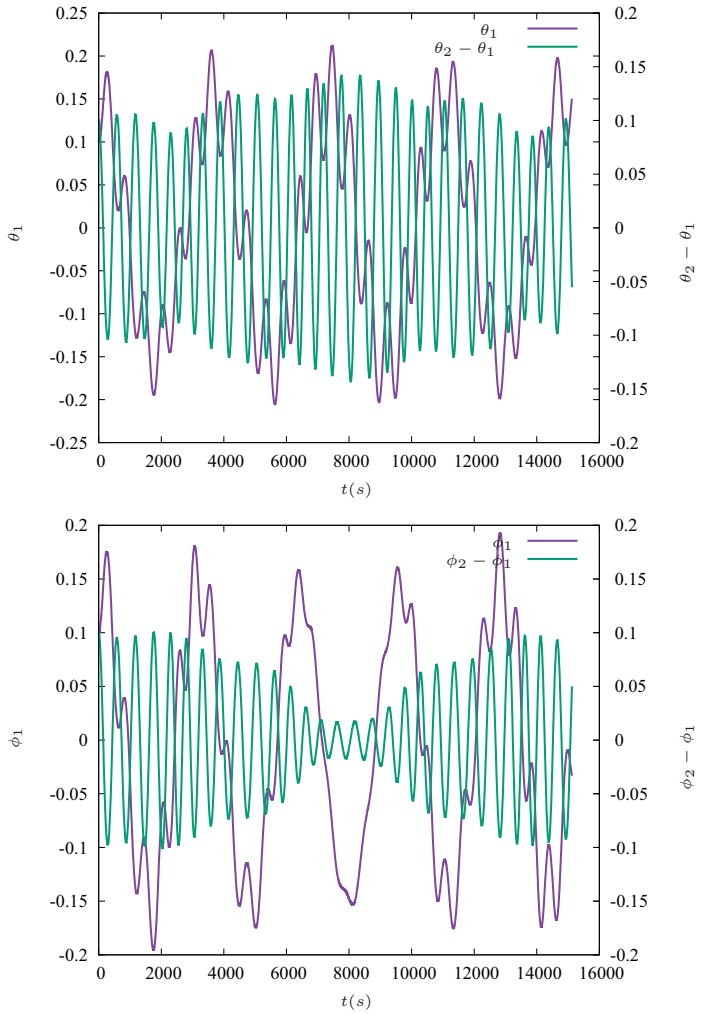

Figure 6. Two bars tether model in circular orbit. Initial conditions: No-straight tether with $\theta_{0,1} = 0.1$, $\theta_{0,1} = 0.2$, $\phi_{0,1} = 0.1$, $\phi_{0,1} = 0.2$

equivalent masses.

The formulation is flexible enough for the simulation of complex multi-tethered systems, with a rigid body as central body.

Based on the Cowell's and DROMO orbit propagators, a set of libraries for general space dynamics applications and space tethers simulation have been developed in the simulation tool EcosimPro, taking advantage of the object-oriented and non-causal modeling capabilities.

Some preliminary test cases have been run, showing good agreement with known results. A deorbiting mission simulation shows that the new tether simulator is a promising tool for the simulation of space tether systems.

Additional test cases are to be presented for the validation of the different capabilities of the simulator (multi-tethered systems, spacecraft attitude coupling), and specifically for the tether lateral dynamics simulation with the new tool.

New modeling capabilities, such as varying length tethers, flexible spacecraft effects, additional perturbing forces or the simulation of the tether system together with other spacecraft systems (electrical, attitude control), will be presented in future works.

7. References

[1] Cartmell, M. and McKenzie, D. "A review of space tether research." Progress in Aerospace Sciences, Vol. 44, No. 1, pp. 1 – 21, 2008. ISSN 0376-0421. doi:DOI:10.1016/j.paerosci.2007.08.002.

[2] Losada, J. R. S., Charro, M., Lorenzini, E. C., and et al. "Bets: Propellant less de orbiting of space debris by bare electrodynamic tethers." 2012.

[3] Zhong, R. and Zhu, Z. "Optimal control of nanosatellite fast deorbit using electrodynamic tether." Journal of Guidance, Control, and Dynamics, 37(4):1182–1194, 2014.

[4] Bombardelli, C., Zanutto, D., and Lorenzini, E. "Deorbiting performance of bare electrodynamic tethers in inclined orbits." Journal of Guidance, Control, and Dynamics, 2013.

[5] Ellis, J. R. and Hall, C. D. "Model Development and Code Verification for Simulation of Electrodynamic Tether System." Journal of Guidance Control Dynamics, 32:1713–1722, November, 2009.

[6] Peláez, J., Hedo, J. M., and de Andrés, P. R. "A special perturbation method in orbital dynamics." Celestial Mechanics and Dynamical Astronomy, Vol. 97, pp. 131–150, Feb. 2007. doi:10.1007/s10569-006-9056-3.

[7] Beletsky, V. V. and Levin, E. M. Dynamics of space tether systems. 1993.

[8] R.Wertz, J. Spacecraft Attitude Determination and Control. Kluwer Academic Publishers, 1978.

[9] Hughes, P. C. Spacecraft attitude dynamics. John Wiley & Sons, New York, 1986.

[10] Battin, R. An Introduction to the Mathematics and Methods of Astrodynamics. AIAA education series. American Institute of Aeronautics & Astronautics, 1999. ISBN 9781600860263.

[11] PA, H. "Auseinandersetzung einer zweckma ssigen mmethod zur berechnung der absoluten sto rungen der kleinen planeten." Abh der Math-Phys Cl der Kon Sachs Ges der Wissensch 5:41218, 1857.

[12] Vázquez, F. Introduction to modelling with ecosimpro. Pearson Educación, 2010. ISBN 9788483226827.

[13] "www.ecosimpro.com."

[14] Moral, J., Rodríguez, F., Vilá, J., Matteo, F. D., and Steelant, J. "1-D Simulation of Solid and Hybrid Combustors with EcosimPro/ESPSS."

[15] Fernandez, A., DAccolti, G., Buergler, B., and Garcia, B. "PEPS. A tool for power system Simulation."

[16] Koppel, C. R., de Rosa, M., Moral, J., and Steelant, J. "A Satellite library in EcosimPro for the AOCS effects on the propulsion subsystem."

[17] Cellier, F. E. and Kofman, E. Continuous System Simulation. 2006.

[18] Stiefel, E. and Scheifele, G. Linear and Regular Celestial Mechanics. Springer, 1971.

[19] Sanjurjo-Rivo, M. Self-Balanced Electrodynamic Tethers. Space Debris Mitigation and other Applications. Ph.D. thesis, Universidad Politécnica de Madrid, 2009.

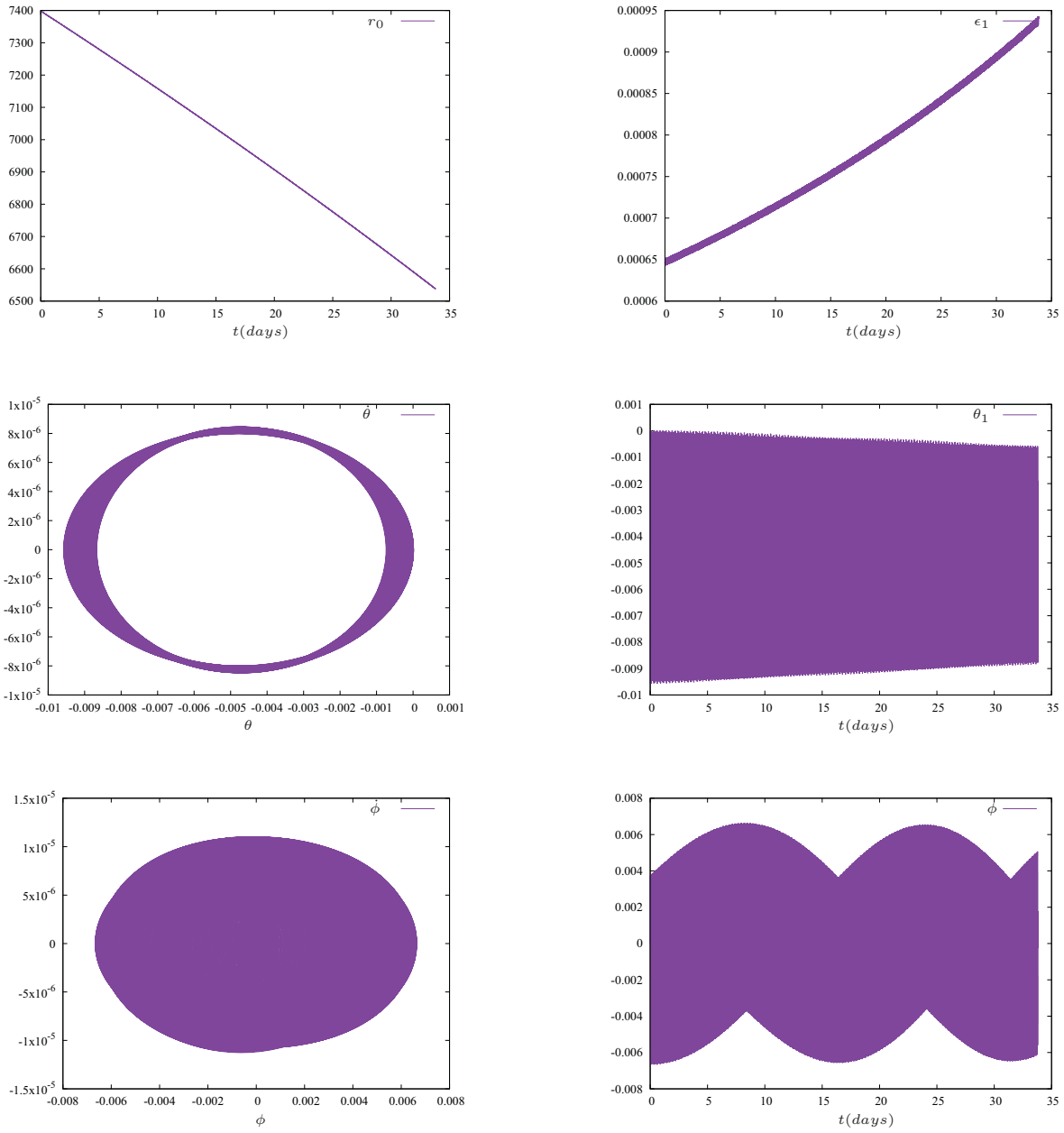

Figure 7. De-orbit mission: simulation results with 1 bar